Chapter 13

Repetitive Nanosecond Volume Discharges under Airflows

Jingfeng Tang, Liqiu Wei and Daren Yu

Additional information is available at the end of the chapter

http://dx.doi.org/10.5772/intechopen.81919

Abstract

Atmospheric pressure discharges are widely used in active airflow control, material synthesis, and air treatment. The key to an optimal application performance lies in how to generate stable and diffuse plasma especially in a large volume and in high-speed airflows. This chapter presents the study of repetitive nanosecond volume discharges under high-speed airflows. The volume discharge strongly depends on the airflows, and the corresponding discharge modes vary from filament to diffuse modes with addition of airflows. The role of airflows provides negative effects on discharge currents as well as discharge densities. Moreover, a type of discharge device with upstream and downstream structure is proposed to demonstrate that charged particles produced by the upstream discharge are transported to the downstream zone and play a pre-ionization and enhanced effect to the downstream discharges.

Keywords: repetitive nanosecond discharges, volume discharges, airflows, upstream and downstream flow

1. Introduction

Recently, atmospheric pressure discharge plasma has been considered for many applications, such as airflow control [1–20], material modification [21–31], air purification [31–49], and so on. With the difference from low-pressure discharge plasmas, atmospheric pressure discharge plasmas are usually operated under an open environment, and the collision between ions and electrons is very frequent. Such strong elastic and/or inelastic collision produces a significant chemical effect and corresponding thermal effect. In addition, air as the media of the discharge process is usually in a flow state, such with an airflow state with different velocities. The various particles in the plasmas always perform a macro-overall movement, and the exchange

of energy and momentum occurs between plasmas and airflows. Therefore, the atmospheric pressure discharge plasma is actually in a typical multi-field couple system, and the coupling interaction between airflows and discharges is of extensive concerns [1].

As the couple interaction between plasmas and airflows, the plasmas macroscopically exhibit a fluid state property, the distribution of plasma particles is influenced by the heat and mass transfer from airflows, and discharge modes and discharge intensities are also changed. As a simultaneous inverse role, the energy release by discharge can cause impulsive interference and thermal effect on airflows, and a change of airflow field distribution can be generated. The airflow transport effect determines the distribution of uncharged particles, and such distribution provides an ionization condition, thus affecting the discharge breakdown. The transfer of heat and mass from airflows provides a new factor on the plasma diffusion, and the discharge energy dissipation and discharge plasmas also provide an active control of airflow distribution. To be sure, discharge plasmas under airflows have undergone a fundamental change. With the presence of airflows, discharge plasmas are more dominant with a strong interaction between plasmas and airflows.

The couple between plasmas and airflows has been considered as the interaction between discharge plasma dynamics and gas dynamics, from a view of time and space scales. For discharge plasmas, the topical time scales include as follows: the establishment of electric field and the generation of plasma (nanoseconds), the dissipation and the quenching of plasma (nanoseconds and/or microseconds), and the life of charged particles (seconds and/or hours). For airflows, the typical time scale is mainly determined by airflow conditions, such as the transport time of airflow (microseconds and/or milliseconds) and the convection heat transfer time (milliseconds and/or seconds) [2]. For discharge plasmas, the typical space scale is about a small size (micrometers and/or millimeters), such as the mean free path and the thickness of plasma sheath. For airflows, the typical space scale is about a big size (millimeters and/or meters), such as the thickness of boundary layer [3]. Under such couple with a multi-time and a multi-space scale, it is necessary to recognize the phenomenon and mechanism of discharges under airflows.

2. Background for discharges under airflows

Plasma flow control is a type of active flow control technology based on discharge plasma technologies, which is advantageous of little power, quick response, and perfect actuation. Russians, Americans, and other research groups [4–20] have done an in-depth study on plasma flow control, as well as the interaction between plasmas and airflows, to improve the aerodynamic characteristics and promote the scientific basis for efficiency. Discharge plasmas applied to flow control mainly include surface discharges [4–14] and volume discharges [15–20]. Surface discharges are used to flow separation control by DBD discharges with a momentum exchange to neutral airflows, which generate a complex pattern of quasi-planar and spherical compression wave [4–8], as well as which are related to a strong demand on stable discharges within the flow boundary layer [7–14]. Volume discharges are applied in MHD flow control to achieve the acceleration and deceleration of airflow, which require

high-intensity volume discharges under airflows condition, as well as which essentially need discharge enhancement methods under MHD airflow environment [15–19].

Plasma material processing is promising for material modification and its industrial applications. Efficient discharges are important demands to realize the surface modification and functional structure construction [21–31]. The moderate power density and the uniform energy distribution are beneficial to material modification. However, under a gas flowing condition, discharges can easily transit from a stable state into an unstable state, which can cause a disaster to the industrial application of plasma material processing. In order to obtain a uniform and stable discharge, discharges under airflows are employed to excite plasmas. Work groups [29] illustrate the surface modification of polyimide films by the discharge under airflow, it is found that the plasma at a homogeneous DBD is evenly distributed than at a filamentary DBD, and by the more efficient introduction of atomic oxygen to the PP surface in the case of homogeneous DBD.

Plasma air purification attracts widespread attention in recent years, mainly related with corona discharges under an air supply channel. Plasma air purification has been developed in many applications, including electrostatic precipitation [32–40], industrial gas exhaust treatment [41–44], and indoor air purification [45–49]. Work groups [35] illustrate that the electric power and the energy loss of corona discharges highly depend on airflow velocities, and corona discharge modes are also related to airflow conditions.

In addition, discharges under airflows are of complicated technical challenges, and the mechanism and its characteristics need a deep and wide investigation.

3. Atmospheric pressure volume discharges under airflows

In order to get a better understanding of airflow effects on volume discharge characteristics, this chapter presents the study of nanosecond pulse volume discharges in high-speed airflows.

3.1. Discharge mode characteristics under airflows

The experimental system is shown in **Figure 1**, which includes an air wind tunnel driven by a fan, a nanosecond pulse generator, discharge system, and measurement system. By changing the speed of the fan, the flow velocity at the end of the wind tunnel can be adjusted with a maximum value of up to 200 m/s. A pitot tube is used to measure the flow velocity of the airflow. The plate-plate electrodes are set in a horizontal and parallel manner. The two electrodes are composed of stainless steel plates with a thickness of 2 mm. The electrode edges were fully polished in order to avoid the point discharge occurring at the electrode edges. The two dielectrics are made of mica with a permittivity $\varepsilon r = 6$ and a thickness of 1 mm. The discharge system is installed at the downstream of subsonic wind tunnel exit with the flow direction perpendicular to the electrode surface. The applied voltage has repetitive pulses with a fixed pulse width of 5 ns and a maximum amplitude of 50 kV with a rise time of 5 ns, corresponding to the frequency ranged from 100 Hz to 3.5 kHz, respectively. The voltage and

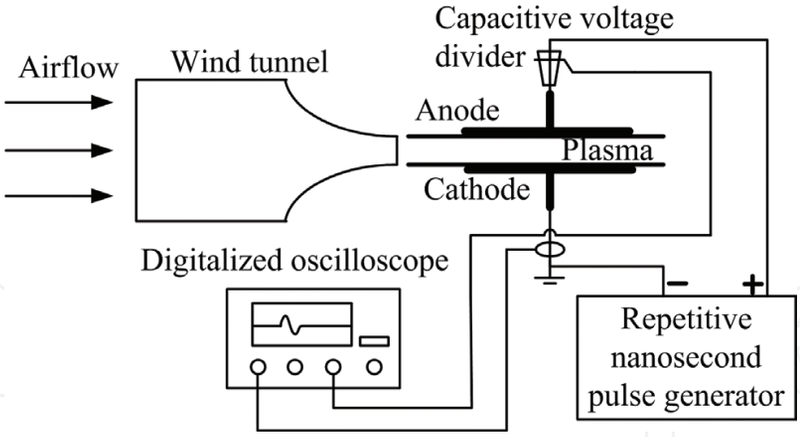

Figure 1. Schematic of experimental setup.

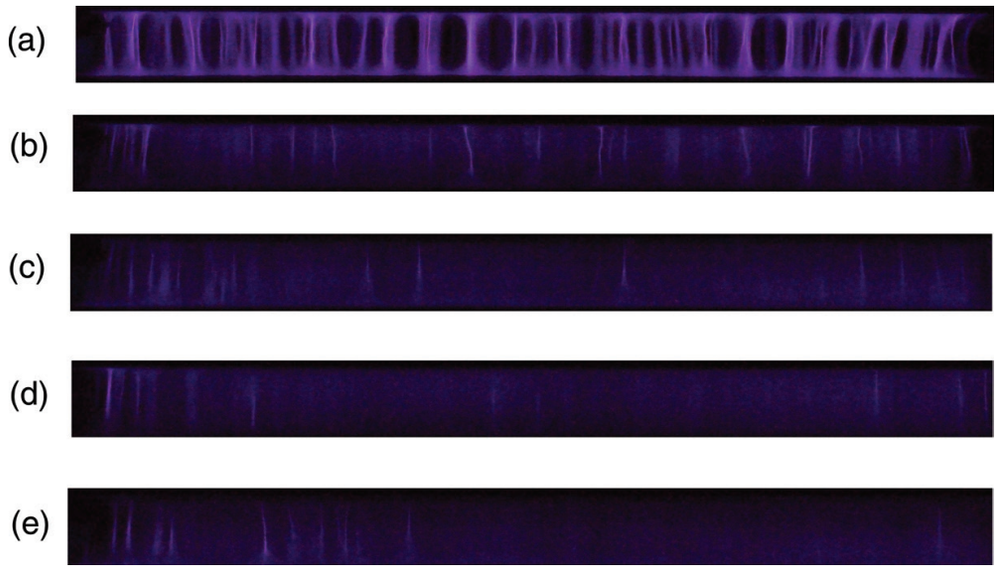

Figure 2. Discharges at different airflow speeds. (a) Flow speed $v = 0$ m/s, (b) $v = 10$ m/s, (c) $v = 35$ m/s, (d) $v = 50$ m/s, and (e) $v = 100$ m/s. Exposure time is 1/1250 s.

current are measured by using a high-voltage probe and a Rogowski coil with a response time of less than 1 ns. The voltage and current signals are recorded by a digitalized oscilloscope with a bandwidth of 1 GHz.

The typical luminous discharge images under airflows are shown in **Figure 2**. In the quiescent air (i.e., the flow velocity is 0 m/s), a multichannel and inhomogeneous violet discharge is present in the discharge volume. The discharge filaments are straight, and the filament foots are randomly and extensively distributed on the dielectric surface, as shown in **Figure 2(a)**. Increasing the flow velocity to 10 m/s, the number of the bright filaments is slightly reduced, but the change of glow component cannot be clearly observed, as shown in **Figure 2(b)**. When the flow velocity varies from 10 to 20 m/s, the filament number is gradually reduced, and the change of discharge luminance and distribution are relatively small. When the airflow with a speed of 35 m/s is introduced into the volume discharge, as shown in **Figure 2(c)**, interestingly, a diffuse discharge in a large volume is promoted. The unsteady nature of the filamentary part of the discharge

cannot be easily observed with the naked eye in the discharge volume. The diffuse and homogeneous discharge mostly occurs at the middle region, and the filament discharge occurs mainly at the inlet region and partly at exit region of the channel. The filament channels on the two sides may be connected to the electric field concentration occurred at electrode edges. With the increasing of airflow speeds, the volume discharge modes vary from filament to diffuse modes. Further improving the airflow speed to 50 m/s, as shown in **Figure 2(d)**, a diffuse discharge also occurs at the middle discharge region, as well as with a reduction of luminous intensity.

Moreover, several excitation conditions are selected for the detailed investigation of airflow effects, in which the applied voltage amplitude is chosen from 10 to 30 kV; PRF is selected from 100 to 3800 Hz, and airflow speed is changed from 0 to 200 m/s, respectively. In a quiescent air or under a low speed, it presents filament and inhomogeneous violet discharges in a large volume, as likely shown in **Figure 2(a)**. At such airflow speeds, the number of the bright filaments is slightly increased with only increasing the applied voltage, as a process of the pinch of several filaments. However, the change of discharges cannot be clearly observed with only changing PRFs. With a speed less than 30 m/s, there are less filaments in the volume, and the change of discharge luminance is relatively small with changing the applied voltages and PRFs. With the airflow speed increasing higher, for example, a speed of 50 m/s as shown in **Figure 2(d)**, the relative uniform discharge in a large volume is promoted. Importantly, the discharge becomes unstable and almost fades away at a PRF less than 220 Hz.

3.2. Discharge density characteristics under airflows

As a nanosecond pulse is applied to a plate-plate gap, initial electrons are accelerated by the electric field, and an avalanche process is followed under the electron multiplication of collision ionization. Fast electrons with high energy can run away from the head of the critical avalanche and dominate in the subsequent development of the critical avalanche. When the head of the critical avalanche reaches near to the anode, a discharge bridge is built up between the two dielectrics as well as electrodes, and a discharge current runs through the gap space, which can be represented as the first pulse current. When the applied pulse is gone, more electrons accumulate in the dielectric surface near the anode, interact with interaction of accumulated positive particles near the cathode, and build up a strong electric field imposed on the discharge space. Such space electric field will induce another avalanche process between the two electrodes, and the second pulse currents arise in our experiments.

With an applied pulse voltage of 18 kV and a pulse repetitive frequency of 1800 Hz, the applied voltage and current waveforms under different airflows are shown in **Figure 3**. It is provided that the plate-plate DBD discharge is characterized by a series of two-stage pulse currents. In contrast with the unipolar pulse of applied voltage, the discharge current behaves bipolar and consists of both positive and negative pulses. The discharge current distributes irregularly, which can be attributed to the random nature of breakdown and complicated dynamics in the air gap.

There is a series of two-stage pulse currents for each nanosecond pulsed discharge. Even considering the existence of discharge delays, the first pulse currents always occur with a same breakdown voltage. Furthermore, it can be drawn from **Figure 4** that the first pulse currents increase first and then reduce with airflow speeds. With the flow speed increasing

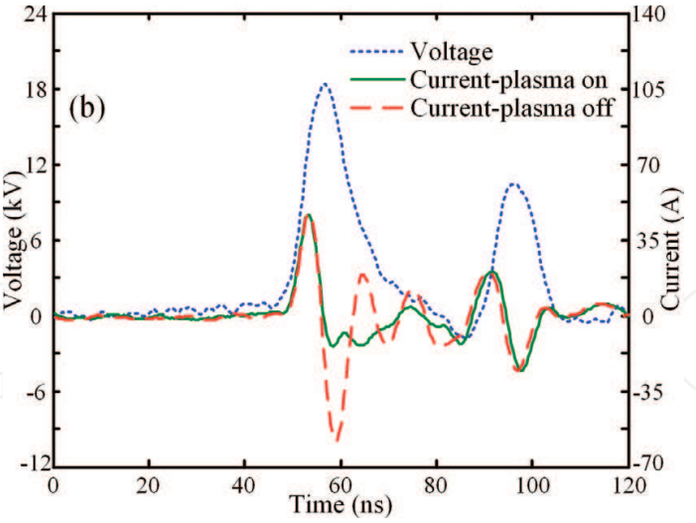

Figure 3. Applied voltage and current waveforms for discharges under airflows.

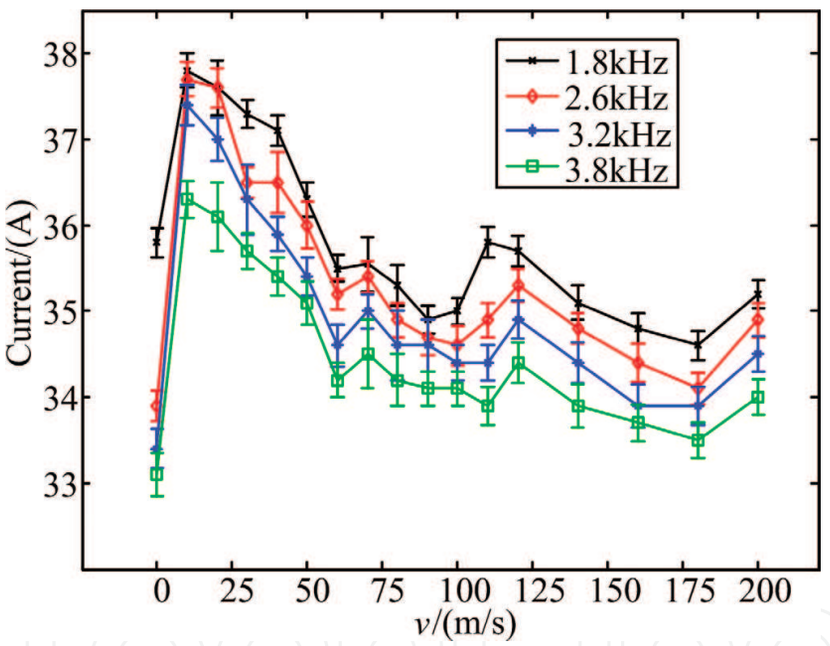

Figure 4. First pulse currents under airflows at different PRFs.

from 0 to 20 m/s, the amplitude of the current rapidly increases from 33.1 to 36.3 A at a PRF of 3800 Hz and then slowly decreases to about 34 A. It goes across a reverse "V"s curve with a turning point at the flow velocity of 20 m/s. The change of first pulse current values imposed by airflows is 4 A. Importantly, there are some factors leading to measurement errors in this works, which mainly include the pressure instability of air supplied to the wind channel, the measurement errors of airflow speed with the pilot tube, and the high frequency noises concerning with nanosecond discharges.

It is clearly shown in **Figure 5** that the second pulse currents are influenced by the addition of airflows to discharge zone. The second pulse currents almost occur at a same time point. At a PRF of 1800 Hz, the second pulse current has a rapid but small change from −34 to −32 A

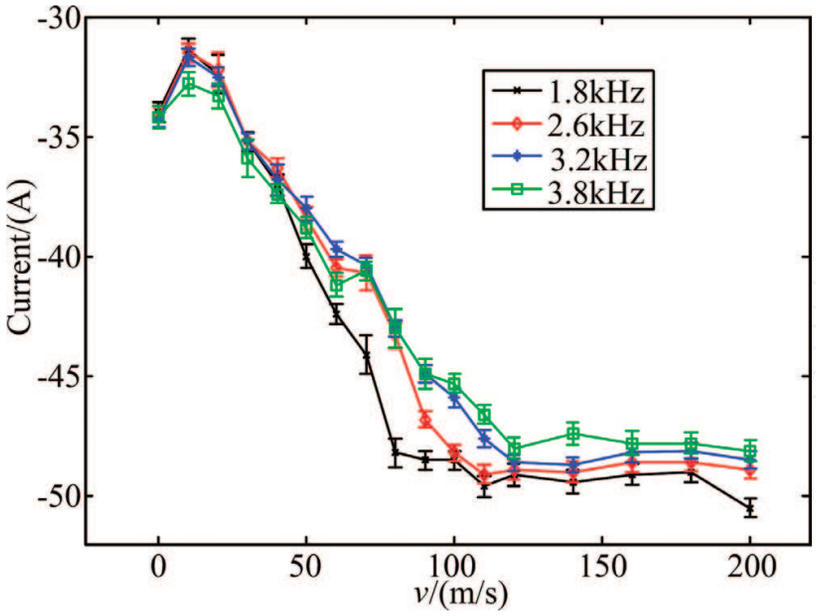

Figure 5. Second pulse currents under airflows at different PRFs.

with the airflow speed increasing from 0 to 20 m/s, follows with a rapid and big change from −32 to −47 A, and then becomes gradually relative stable as the airflow speed is bigger than 80 m/s. It is mostly concerned that the difference between second pulse current values is about 20A for different airflows.

With the airflow added into the gap space, the volume discharge modes vary from filament to diffuse modes, and the induced two-stage pulse currents are also influenced. These behaviors may be attributed to the combined action of two effects. On one hand, the airflows breathe more species into the discharge volume from upstream to downstream, especially the excited metastable state, which causes a decrease in the number of initial electrons. On the other hand, the airflows remove accumulated charges on the surface of the dielectric, which is favorable for the development of discharge.

As the first pulse current is arising, a bigger voltage pulse with a 5 ns rise time, as well as a stronger electric field, is being imposed on the electrodes as one discharge driver. Since the pulse action time is too small, airflows in this period can be considered as "frozen" and without any flow mobility. Therefore, the first pulse currents nearly maintain consistency for different airflow speeds. However, at the second pulse current arising, accumulated particles near the electrodes induce a space electric field as another discharge driver. Since this driver always acts for several milliseconds, airflow mobility must be considered in this period. As indicated in **Figure 5**, the second pulse currents for quiescent air are bigger than that of airflows with speeds less than 40 m/s. Since airflows breathe more species, especially under excited metastable states, out of the discharge volume, the loss of heavy particles under the force of airflows is unfavorable for the development of discharge. Under airflows with a speed of more than 40 m/s, the second pulse currents are always bigger than that of quiescent air. It is concerned with the distribution change of the accumulated charges on the surface of the dielectrics by the force of airflows, which is favorable for the development of discharge. With the speed increasing to more than 80 m/s, the second pulse currents become

gradually relatively stable, which seems unaffected by airflows. The detailed effects under such high airflow speeds are very interesting and are also taken into considerations in the future works.

3.3. Conditional boundary characteristics under airflows

The boundary conditions of DBD volume discharges under airflows velocities are investigated. With the addition of airflows, no matter for any voltage, both the initiation and the extinction pulse repetition frequency need to be kept to a specified value to maintain the presence of discharge. Under a particular applied voltage and when the pulse repetitive frequency is rather low, any discharge does not occur; nevertheless, a current is detected due to the existence of the displacement electric field. With the growth of pulse repetitive frequency, the discharge can be established with an obvious change of discharge current.

The initiation and extinction boundaries are identified by making a subtraction of detected currents between discharge on and off, as shown in **Figures 6** and **7**. To improve the accuracy, the airflow and the applied voltage are kept constant as soon as possible while with an adjustable PRF, and all data are acquired with 10 times measuring. As the airflow velocity accelerates, the initiation and extinction value of PRFs is increased. In a still air, when the applied voltage reaches to 17 kV, the corresponding PRFs needed to reach about 1 kHz, which is almost an order of magnitude larger than the value under 27 kV. The lower is the applied voltage, the larger are the needed PRFs as well as the difference of PRFs. The initiation and extinction PRFs are almost inversely proportional to the applied voltage value under a certain airflow velocity. Once the airflow velocity attains 100 m/s under 17 kV, the discharge is not detected even though the PRF is up to the maximum value of applied value. As a special case of contrast, the initiation and extinction PRFs show a slight dependence on the velocities

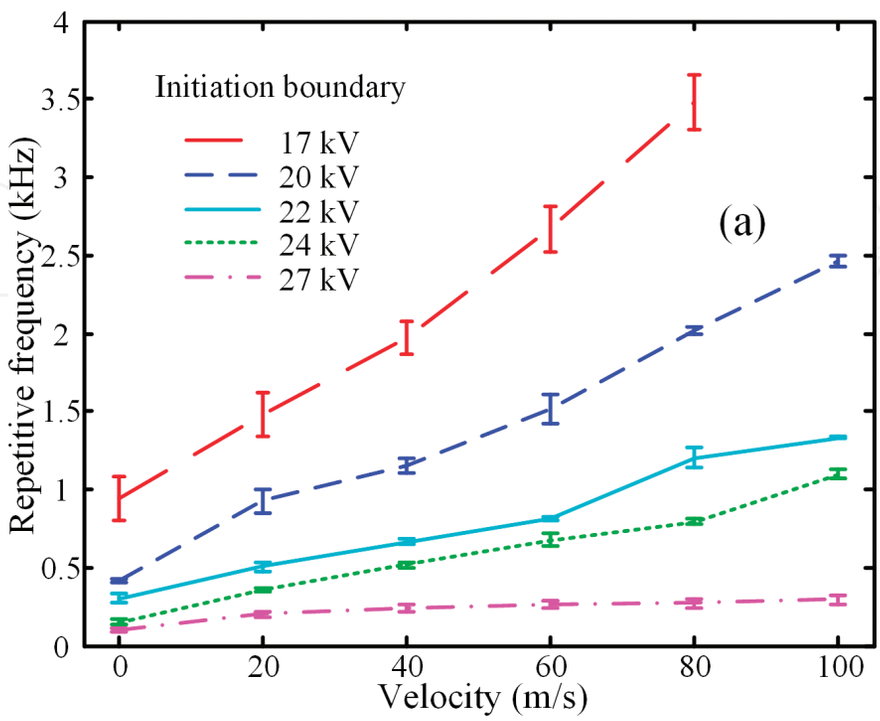

Figure 6. Initiation frequencies versus airflow speeds.

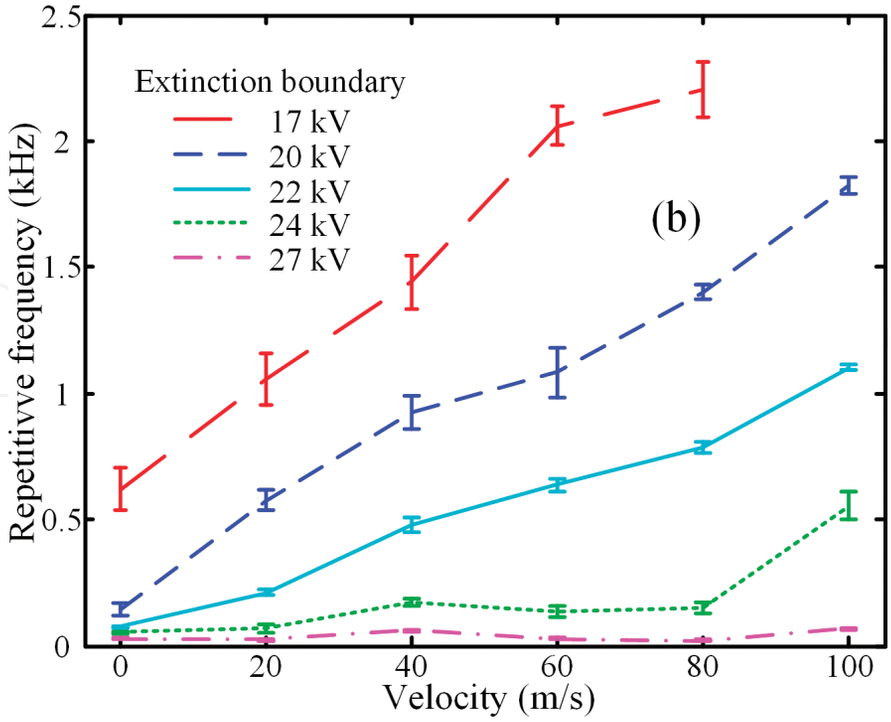

Figure 7. Extinction frequencies versus airflow speeds.

under an applied voltage of 27 kV. It can be concluded that the boundary PRFs are decided by the combined action between the applied voltages and the injected airflows.

In still air, mostly free electrons move rapidly toward the anode under the applied electric field. Many ions and metastable particles are produced by the complicated collisions between various particles in the discharge zone. Considering the interval time between two voltage pulses, only metastable particles with a lifetime of the order of several seconds can survive as residual seeds, while most ions have quenched. So, the increase of PRF can raise the concentration of residual seeds, which make the discharge breakdown more easily to occur. With the addition of the airflows, a large number of seeds are blown away from the discharge region, which makes a difficulty on the next pulsed discharge as well as leads to a growth of initiation PRFs. However, with the applied voltage growing, the free electrons obtain more energy from the electric field, and seed particles deposit on the dielectric plate. Owing to the existence of the viscous boundary layer, the seed particles are hardly moved away by the airflows. As a result under 27 kV, only a slight dependence of the initiation and extinction PRFs is observed with the airflow velocities.

4. Atmospheric pressure volume discharges under upstream and downstream airflows

The previous chapters demonstrate that the volume discharge mode is influenced by airflows and the discharge intensity decreases with the increase of airflow velocities. In this chapter, a type of discharge device with an upstream and downstream structure is provided to investigate the interactions between airflows and discharges. The upstream and downstream discharges under airflow include the generation and transport of charged particles.

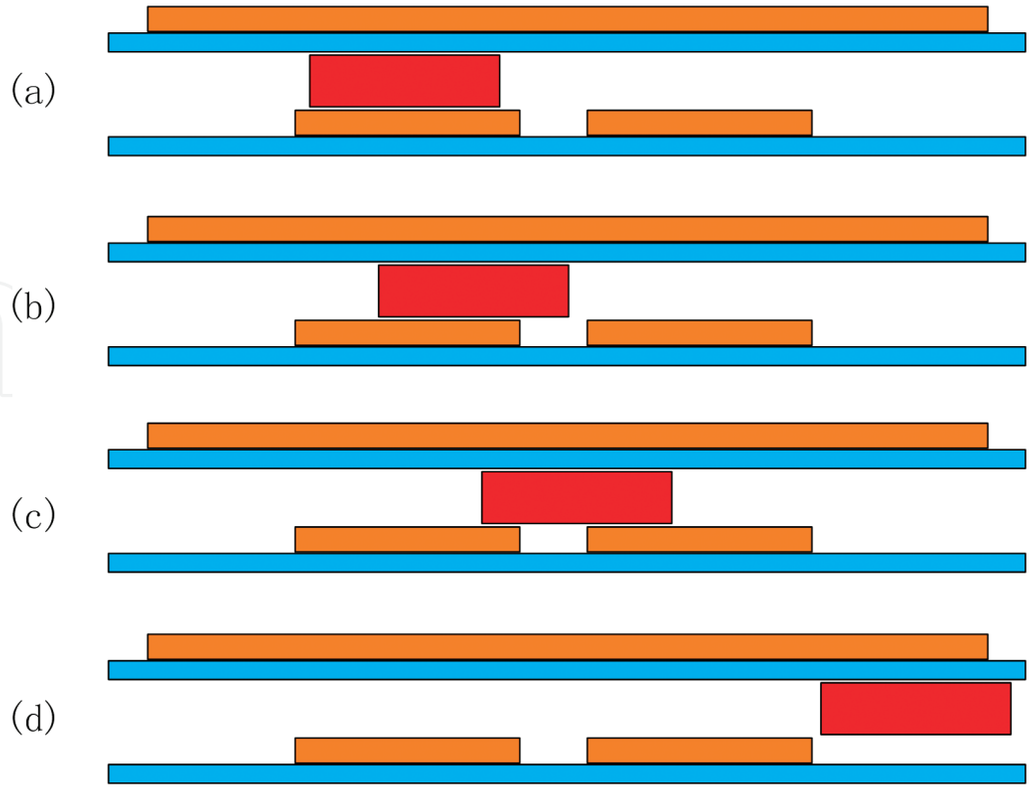

Figure 8. Schematic of discharges under upstream and downstream constructure with different airflow velocities.

The generation of charged particles is related to external pulse excitation, and the transport of particles can be influenced by the effect of airflow. Furthermore, the upstream and downstream discharge in the airflow channel is a multi-time scale problem, including the transport time of airflow and the time of charged particle generation. The characteristic time of airflow is related to the movement path and the airflow velocity, and the generation of particles is adjusted by the repetition frequency of the discharge.

By matching the transport effect of airflow and the pre-ionization of charged particles, some of the particles generated by the upstream discharge are transported to the downstream region, and those particles play a pre-ionization role in the downstream discharge, which causes the enhancement of the downstream discharge intensity. For the purpose of further recognizing the relationship between upstream and downstream discharge under airflow, the behavior of the particles were analyzed as schematically shown in **Figure 8**. In the quiescent air, the discharge products always stay only in the upstream zone, as shown in **Figure 8(a)**; as the airflow is injected, the discharge products produced by upstream zone will be transported to the downstream zone, as shown in **Figure 8(b)** and **8(c)**; as the further increasing of airflow velocity, the discharge product will be blow out the downstream zone, as shown in **Figure 8d**.

The time range of air flow transport time t_f is derived as Eq. (1). By properly controlling the pulse repetition interval time t_p and the air flow transport time t_f, the charged particles could be transported from upstream region to the downstream region and enhance the downstream discharge intensity:

$$L/v <= t_f <= (L + 2^* S)/v \tag{1}$$

where the pulse interval time is denoted as t_p, the distance between the upstream and downstream regions is L, the width of the electrode plate is S, and the airflow velocity is v (m/s).

4.1. Discharge mode characteristics under upstream and downstream airflows

With a pulse repetitive frequency of 1000 Hz, the applied voltage and current waveforms of the DBD volume discharge can be detected, which has been descripted in Section 3.1. By changing the air velocity, the discharge mode characteristics under different airflow velocities are shown in **Figure 9**.

For discharge in a static condition, as shown in **Figure 9(a)**, the upstream and downstream discharge exhibits a filament discharge mode. In the middle region of the electrode, the filaments exhibit a vertical distribution, and the path of the filaments close to the edge of the electrode shows a curved state because of the edge effect of the metal electrode.

For $t_f > t_p$, the discharge filaments move along the direction of flow, the filament path changes from the original vertical state to the curved state along the direction of airflow, and some parts of the discharge area become uniform. The result is shown in **Figure 9(b)**.

For $t_f \leq t_p$, with increasing airflow velocity, most of the discharge area exhibits a uniform state, and the paths of the discharge filaments at the edge of the metal electrodes are attracted by the central discharge region. The discharge filaments shrink to the inside region of discharge, and the discharge region exhibits a pinched state, as shown in **Figure 9(c)** and **(d)**.

4.2. Discharge spectrum characteristics under upstream and downstream airflows

The normalized emission spectra for the upstream and downstream discharges are provided as **Figure 10**. Due to the weak luminescence intensity of volume discharges, the spectrometer exposure time was set to 2 s, which means that the emission intensity was averaged temporally and spatially for 2000 cycles.

With increasing airflow velocity, the intensity of the upstream discharge emission spectrum decreases, which corresponds to a decrease in discharge intensity. As for downstream

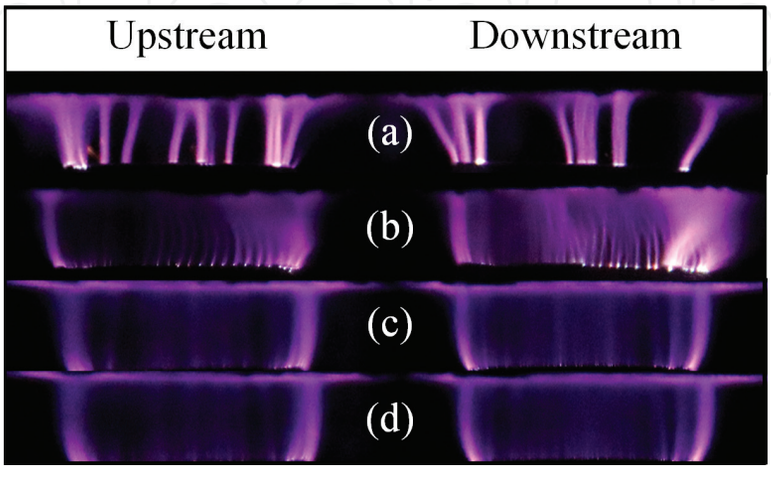

Figure 9. Discharge at different airflow velocities: (a) static air, (b) low speed ($t_f > t_p$), (c) medium speed ($t_f = t_p$), and (d) high speed ($t_f < t_p$).

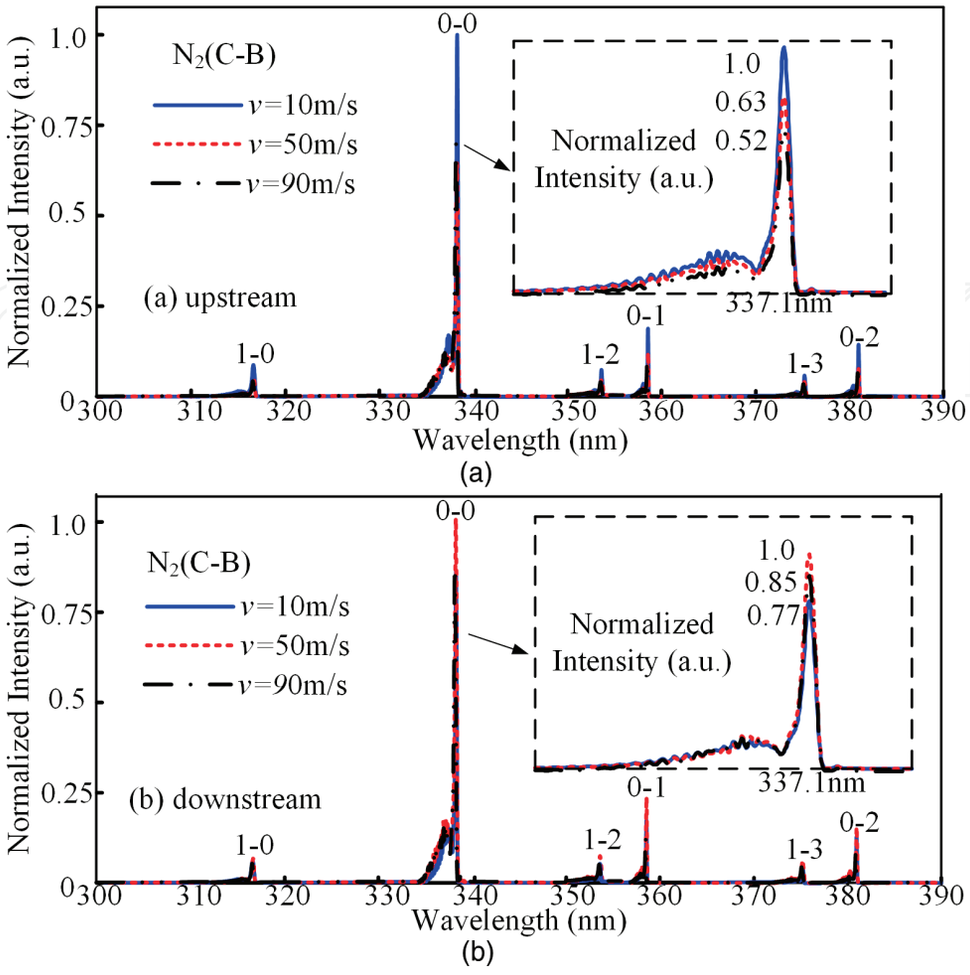

Figure 10. Normalized intensity discharge at different velocities: (a) upstream and (b) downstream.

discharge, when $t_f = t_p$, the intensity of the emission spectrum increases, which proves that the concentration of charged particles in the downstream region increased. At $t_f < t_p$ and $t_f > t_p$, the corresponding spectral intensity gradually decreases.

The dependence of rotational temperature of the upstream and downstream discharges on airflow rates is shown in **Figure 11**. It can be seen that the rotational temperature is approximately 390 K when the discharge is excited in the static air. The rotational temperature decreases to approximately 320 K as the airflow velocity increases gradually to 80 m/s. The low gas temperature may be attributed to two reasons. One is that the duty cycle of the pulse power supply is low; another is that more energy is delivered to the energetic electrons. The gas temperature is substantially the same in the upstream and downstream regions. This result shows that the gas temperature under airflow is not the key factor that causes the difference between the upstream and downstream discharge intensity.

Under the condition of reasonable matching between t_f and t_p, the mass transfer effect of airflow plays a dominant role in the upstream and downstream discharges. The particles generated by the upstream discharge can be transported to the downstream discharge region. The combined effect of flow transport and pre-ionization of charged particles enhances the downstream discharge.

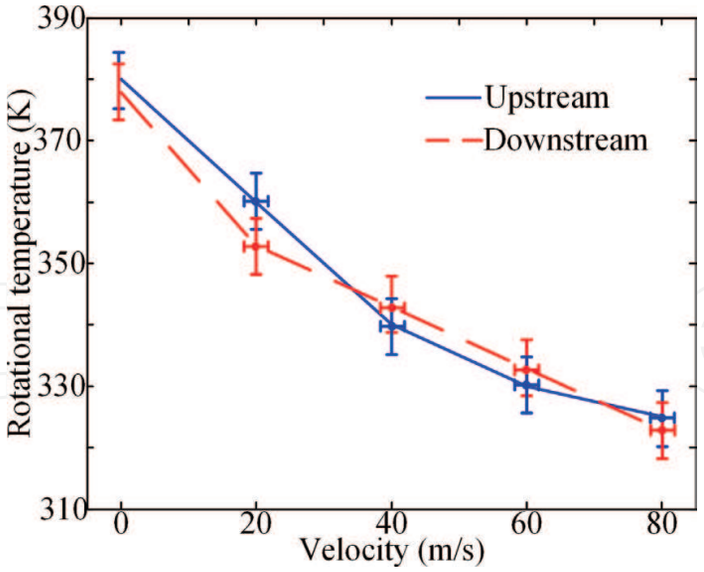

Figure 11. Rotational temperature at different velocities.

4.3. Discharge difference between upstream and downstream region

4.3.1. Various airflow velocities

The comparison of discharge currents between upstream and downstream discharges is shown in **Figure 12**. The current peak is used to illustrate the discharge intensity under different flow velocities.

For $t_f > t_p$, the amplitude of the upstream discharge decreases from 55 to 53 A, and the downstream discharge fluctuates between 38 and 36 A with increased airflow speed, and for the condition of $t_f = t_p$, the amplitude of the upstream discharge gradually decreases from 53 to 45 A. For the downstream discharge, the amplitude exhibits an opposite trend, changing from 36 to 46 A. With increasing airflow velocity, the amplitude of the upstream discharge current continues to decrease, and the increasing rate of the downstream discharge current tends to be zero.

4.3.2. Various PRFs

The pulse frequencies were adjusted to f = 2 kHz and f = 200 Hz, and the results are shown in **Figure 13**. When the pulse frequency is 2 kHz, for $t_f > t_p$, the current amplitudes of the upstream discharge gradually decrease from 59 to 57 A, and the downstream discharge fluctuates between 45 and 48 A. When the airflow velocity increases until $t_f = t_p$, the amplitude of the upstream discharge gradually decreases from 57 to 49 A. The amplitude of the downstream discharge exhibits an opposite trend and increases from 48 to 56 A.

When the discharge frequency was adjusted to 200 Hz, the pulse interval time t_p was 5 ms. Because of the low pulse repetition frequency, the charged particles in the space completed the diffusion and recombination process within the pulse interval time, causing the reduction in discharge intensity. In the meantime, at a lower airflow velocity ($t_f > t_p$), the amplitude of

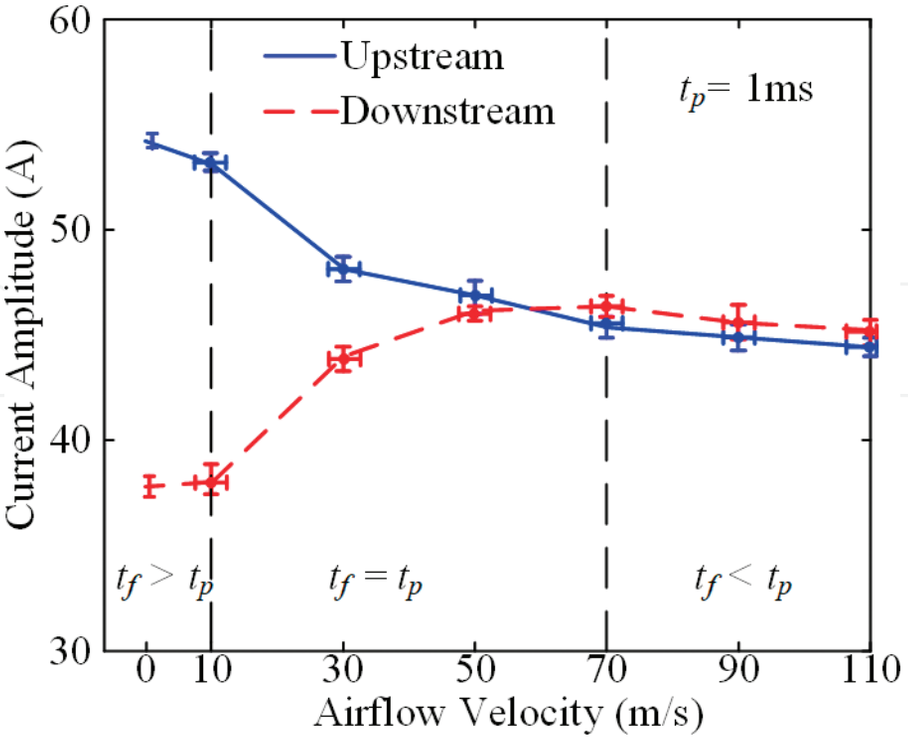

Figure 12. Discharge current amplitude of the upstream and downstream regions.

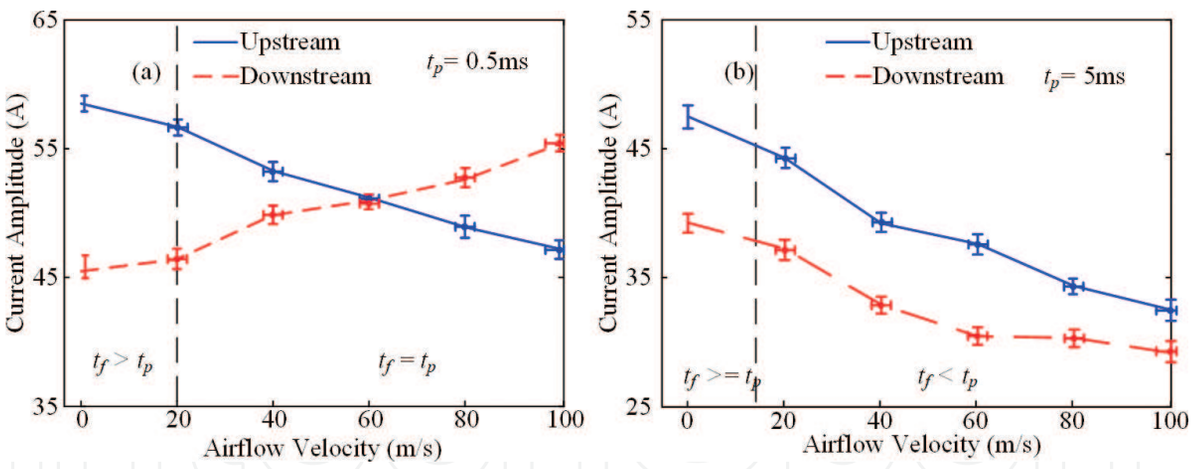

Figure 13. Discharge current amplitude at different PRFs: (a) PRF = 2 kHz and (b) PRF = 200 Hz.

the discharge current in the upstream region attenuated from 44 to 35 A, and the downstream discharge current weakened from 38 to 30 A.

4.3.3. Various distances between upstream and downstream

The conditions of L = 20 mm and L = 50 mm were studied. The experimental results for f = 1 kHz are shown in **Figure 14**. When the discharge electrode spacing was adjusted to L = 20 mm, for $t_f > t_p$, the charged particles generated by the upstream discharge could not transit to the downstream discharge region. The peak value of the upstream discharge current decayed from 54 to 50 A, and the amplitude of the downstream discharge current fluctuated between 37 and 39 A. During the

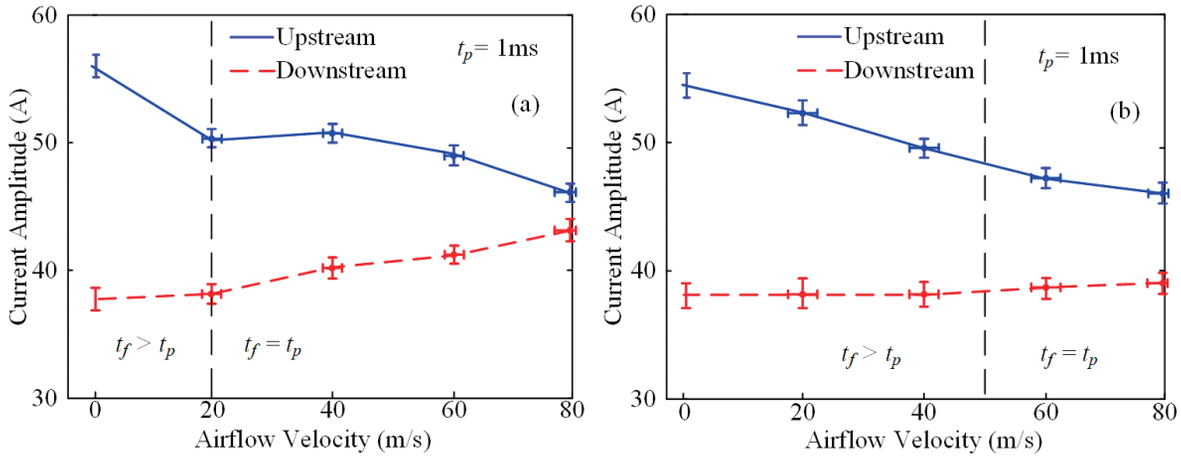

Figure 14. Discharge current amplitude at different distances: (a) L = 20 mm and (b) L = 50 mm.

process of increasing airflow velocity until $t_f = t_p$, particles generated in the upstream discharge region were blown to the downstream discharge region. The peak value of the upstream discharge current decayed gradually from 50 to 45 A, and the corresponding downstream discharge current amplitude gradually increased to 43 A. When the electrode spacing was adjusted to 50 mm, with the gas velocity reaching 50 m/s (i.e., $t_{f1} = t_p$), the particles generated in the upstream discharge region could be transported to the downstream discharge region. The upstream and downstream discharge currents are almost enhanced with the increased gas flow velocity.

4.4. Interaction between upstream and downstream discharges

According to the process of pulse discharge, the electrons move to the anode under the effect of pulse voltage, and the ions remain nearly static in the time scale of nanoseconds; the discharge current is formed by electron migration. The electrons cover the surface of the dielectric, and a large amount of ions are accumulated in the discharge space. At the falling edge of the voltage pulse, when the applied voltage potential is lower than the potential generated by the positive charge space, some electrons move toward the cathode and form a reverse current. During the movement, the electrons are neutralized with some positive ions, and the concentration of positive charges declines in the space.

Because of the different time scales of pulse discharge and airflow, the airflow cannot directly affect the process of pulse discharge. The rising time of the pulse discharge takes place in a few nanoseconds, and the duration of current is in the tens nanoseconds. For particles, the diffusion and recombination of neutral and charged particles take place on a micro- and millisecond time scale, and the lifetime of the metastable particles produced by the discharge in short gaps is thought to have a significant high concentration of some hundreds of microseconds to milliseconds. Therefore, the airflow can affect only the discharge distribution of particles during the pulse interval times.

When the airflow is applied in the discharge space, the distribution and movement of particles in the discharge region could be influenced by the airflow; a schematic of the particle motion paths is shown in **Figure 15**, and the analysis is as follows.

Metastable particles are transported by the drag force of the airflow and move from the upstream discharge area to the downstream discharge area, which particles play the pre-ionization role to

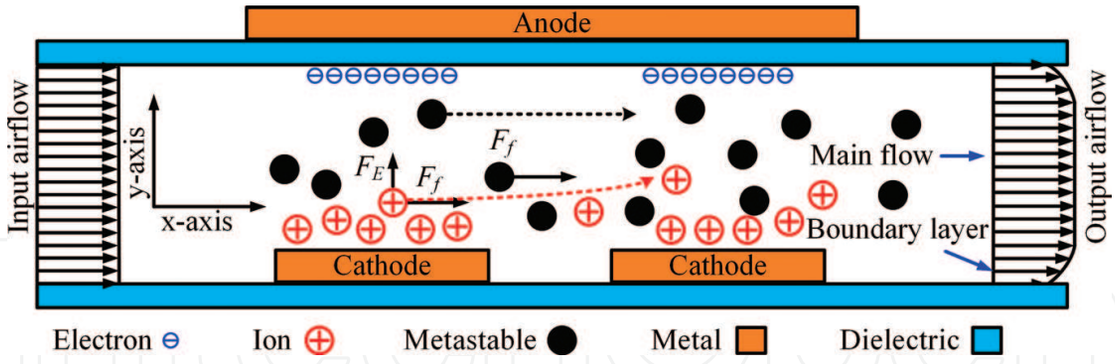

Figure 15. Schematic of particle motion paths.

the downstream discharge. For the charged ions in space, the ions move along the airflow direction mainly under the effect of the drag force of airflow and the electrostatic force from the surface electrons [15, 16]. According to the literature, during a pulse interval time of approximately 1 ms, the electric field strength between the surface electrons and the space charges is several kV/cm, and the ion density n_i is approximately 10^{12} cm^{-3}. The estimated electric field force of the ions is approximately 1.6×10^{-2} N. In terms of the bulk flow, the conservation of momentum of the bulk fluid is described by the Navier-Stokes equation. The air density is approximately 1.29 kg/m^3, the volume of the discharge area is approximately 5 mm × 30 mm × 30 mm, and the pressure difference between inlet and outlet is nearly 0.5% of the atmospheric pressure. The estimated flow field force to the ions is approximately 1.2×10^{-1} N, and the ratio of the flow force and the electrical field force is approximately 8:1. For the ions in the gap, the distance of ions moved along the y-axis is approximately 2 mm during a pulse interval of 1 ms, which is less than the gap distance. The estimation illustrates that the ions are blown to the downstream area during the pulse interval time under the coupling force of the airflow and electric field.

Furthermore, the space charges have different velocities at different regions in the airflow channel. In the region near the dielectric, the space charges have a lower velocity because of the drag force in the boundary layer and the larger electrostatic force from the surface charges. However, the space charges in the middle region of the gap have the fastest velocities and the smaller electrostatic force, and the drag force from the airflow plays a dominant role compared with the electrostatic force of the surface electrons. The curved discharge channel under the low-speed condition also illustrates that the effect of the drag force from the mainstream area is stronger than the electrostatic force between the surface electrons and the space charges; this phenomenon is also discussed in the literature [15, 22]. Therefore, both the estimation results and the discharge phenomenon illustrate that some particles, such as metastable particles and ions, could transit to the downstream discharge area during the pulse interval time; these particles act as seed electrons to the downstream discharge, and the downstream discharge intensity is enhanced.

Acknowledgements

Parts of this chapter source from authors' recent work [50, 51]. The authors thank to PhD student Zhou Desheng and Tang Miao to provide the experimental materials for the book. The authors would like to acknowledge the support of the National Natural Science Foundation of China (no. 51437002).

Author details

Jingfeng Tang, Liqiu Wei* and Daren Yu

*Address all correspondence to: weiliqiu@hit.edu.cn

Harbin Institute of Technology, Harbin, People's Republic of China

References

[1] Starikovskiy A, Aleksandrov N. Nonequilibrium Plasma Aerodynamics. Rijeka: In Tech; 2011. pp. 55-96

[2] Zheng JG, Zhao ZJ, Li J, et al. Numerical simulation of nanosecond pulsed dielectric barrier discharge actuator in a quiescent flow. Physics of Fluids. 2014;**26**(3):036102

[3] Kriegseis J, Grundmann S, Tropea C. Airflow influence on the discharge performance of dielectric barrier discharge plasma actuators. Physics of Plasmas. 2012;**19**(7):073509

[4] Adamovich IV, Little J, Nishihara M, et al. Nanosecond pulse surface discharges for high sped flow control, AIAA 2012 3137. Reston: AIAA; 2012

[5] Bletzinger P, Ganguly BN, van Wie D, et al. Plasmas in high speed aerodynamics. Journal of Physics D: Applied Physics. 2005;**38**(4):33-57

[6] Moreau E. Airflow control by nonthermal plasma actuators. Journal of Physics. D, Applied Physics. 2007;**40**(3):605-636

[7] Boeuf JP, Pitchford LC. Electrohydrodynamic force and aerodynamic flow acceleration in surface dielectric barrier discharge. Journal of Applied Physics. 2005;**97**(10):103307

[8] Font GI, Morgan WL. Recent progress in dielectric barrier discharges for aerodynamic flow control. Contributions to Plasma Physics. 2007;**47**(12):103-110

[9] Corke TC, Enloe CL, Wilkinson SP. Dielectric barrier discharge plasma actuators for flow control. Annual Review of Fluid Mechanics. 2010;**42**:505-529

[10] Li YH, Wu Y, Song HM, et al. Plasma Flow Control. Rijeka: InTech; 2011. pp. 21-54

[11] Nie WS, Cheng YF, Che XK. A review on dielectric barrier discharge plasma flow control. Advances in Applied Mechanics. 2012;**42**(6):722-734

[12] Riherd M, Roy S. Serpentine geometry plasma actuators for flow control. Journal of Applied Physics. 2013;**114**(8):083303

[13] Wu Y, LiY H, Jia M, et al. Influence of operating pressure on surface dielectric barrier discharge plasma aerodynamic actuation characteristics. Applied Physics Letters. 2008;**93**(3):031503

[14] Che XK, Shao T, Nie WS, et al. Numerical simulation on a nanosecond pulse surface dielectric barrier discharge actuator in near space. Journal of Physics. D, Applied Physics. 2012;**45**(14):145201

[15] Murakamia T, Okuno Y. Experiments and numerical simulations on high-density magnetohydrodynamic electrical power generation. Journal of Applied Physics. 2008; **104**:063307

[16] Lee CH, Lu HY. Quasi-one-dimensional parametric study for MHD generator in MHD bypass scramjet system. In: AIAA Paper 2007-644

[17] Bityurin VA. A feasibility study and experimental evaluation on MHD acceleration for application to advanced propulsion and hypervelocity ground testing. In: AIAA Paper 2000, 2301

[18] Su CB, Li YH, Cheng BQ. Experimental investigation of MHD flow control for the oblique shockwave around the ramp in low-temperature supersonic flow. Chinese Journal of Aeronautics. 2010;**22**:22-32

[19] Fujino T, Sugita H, Mizuno M. Influences of electrical conductivity of wall on magnetohydrodynamic control of aerodynamic heating. Journal of Spacecraft and Rockets. 2006;**43**:63-70

[20] Benard N, Moreau E. E H D force and electric wind produced by surface dielectric barrier discharge plasma actuators used for airflow control. In: AIAA 2012 3136. Reston: AIAA; 2012

[21] Hiraoka H, Lazare S. Surface modifications of kapton and cured polyimide films by Arf excimer laser—Applications to imagewise wetting and metallization. Applied Surface Science. 1990;**46**(1-4):264-271

[22] Sung K, Hwang SM, Lee CM, et al. Effects of chemical etching and functionalization times on the properties of Cu/polyimide films. Journal of the Korean Physical Society. 2010;**57**(6):1707-1712

[23] Noh BI, Yoon JW, Jung SB. Effect of laminating parameters on the adhesion property of flexible copper clad laminate with adhesive layer. International Journal of Adhesion and Adhesives. 2010;**30**(1):30-35

[24] Shin JW, Jeun JP, Kang PH. Surface modification and characterization of N+ ion implantation on polyimide film. Macromolecular Research. 2010;**18**(3):227-232

[25] Miron C, Sava I, Jepu I, et al. Surface modification of the polyimide films by electrical discharges in water. Plasma Processes and Polymers. 2013;**10**(9):798-807

[26] Chung TS, Shao L, Tin PS. Surface modification of polyimide membranes by diamines for H-2 and CO_2 separation. Macromolecular Rapid Communications. 2006;**27**(13):998-1003

[27] Park SC, Youn SW, Takagi H, et al. A study on surface modification of soluble block copolymer polyimide by UV irradiation and its application to electroless plating. Journal of Photopolymer Science and Technology. 2013;**26**(3):297-302

[28] Shao T, Zhang C, Long KH, et al. Surface modification of polyimide films using unipolar nanosecond-pulse DBD in atmospheric air. Applied Surface Science. 2010; **256**(12):3888-3894

[29] Fang Z, Xie Z, Li J, et al. Comparison of surface modification of polypropylene film by filamentary DBD at atmospheric pressure and homogeneous DBD at medium pressure in air. Journal of Physics D: Applied Physics. 2009;**42**:085204. 9 pp

[30] Park SC, Yoon SS, Nam JD. Surface characteristics and adhesive strengths of metal on O-2 ion beam treated polyimide substrate. Thin Solid Films. 2008;**516**(10):3028-3035

[31] Bulycheva NA, Kazaryana MA, Chaikov LL, et al. Nanoscale metal oxide particles produced in the plasma discharge in the liquid phase upon exposure to ultrasonic cavitation. 1. Method for producing particles. Bulletin of the Lebedev Physics Institute. 2014;**41**(9):264

[32] Hao Y, Wenchun W, Dezheng Y, et al. Atmospheric air dielectric barrier discharge excited by nanosecond pulse and AC used for improving the hydrophilicity of aramid fibers. Plasma Science and Technology. 2017;**19**:125401. 9 pp

[33] Zouaghi A, Mekhaldi A. Analysis of nanosecond pulsed and square AC dielectric barrier discharges in planar configuration: Application to electrostatic precipitation. IEEE Transactions on Dielectrics and Electrical Insulation. 2017;**24**(4)

[34] Athanasios CM, Igor VT, et al. Superposition of DC voltage and submicrosecond impulses for energization of electrostatic precipitators. IEEE Transactions on Plasma Science. 2012;**40**(10)

[35] Sato S, Kimura M, et al. A removal system of diesel particulate using electrostatic precipitator with discharge plasma. In: IAS. 2005. pp. 2203-2206

[36] Lee YH, Jung WS, Choi YR, et al. Application of pulsed corona induced plasma chemical process to an industrial incinerator. Environmental Science & Technology. 2003; **37**(11):2563

[37] Chang JS, Urashima K, Tong YX, et al. Simultaneous removal of NO_x and SO_2 from coal boiler flue gases by DC corona discharge ammonia radical shower systems: Pilot plant tests. Journal of Electrostatics. 2003;**57**(3-4):313

[38] Chang MB, Kushner MJ, Rood MJ. Removal of SO_2 and the simultaneous removal of SO_2 and NO from simulated flue gas streams using dielectric barrier discharge plasmas. Plasma Chemistry and Plasma Processing. 1992;**12**(4):565

[39] Obradović BM, Sretenović GB, Kuraica MM. A dual-use of DBD plasma for simultaneous NO_x and SO_2 removal from coal-combustion flue gas. Journal of Hazardous Materials. 2011;**185**(2-3):1280

[40] Masuda S, Hosokawa S, Tu X, et al. Novel plasma chemical technologies-PPCP and SPCP for control of gaseous pollutants and air toxics. Journal of Electrostatics. 1995;**34**(4):415

[41] Fan X, Zhu T, Sun Y, et al. The roles of various plasma species in the plasma and plasma-catalytic removal of low-concentration formaldehyde in air. Journal of Hazardous Materials. 2011;**196**:380

[42] Zhang X, Feng F, Li S, et al. Aerosol formation from styrene removal with an AC/DC streamer corona plasma system in air. Chemical Engineering Journal. 2013;**232**:527

[43] Harling A, Glover DJ, Whitehead JC, et al. Novel method for enhancing the destruction of environmental pollutants by the combination of multiple plasma discharges. Environmental Science & Technology. 2008;**42**(12):4546

[44] Zhu T, Wan Y, Li H, et al. VOCs decomposition via modified ferroelectric packed bed dielectric barrier discharge plasma. IEEE Transactions on Plasma Science. 2011;**39**(8):1695

[45] Dou B, Bin F, Wang C, et al. Discharge characteristics and abatement of volatile organic compounds using plasma reactor packed with ceramic Raschig rings. Journal of Electrostatics. 2013;**71**(5):939

[46] Zheng C, Zhu X, Gao X, et al. Experimental study of acetone removal by packed-bed dielectric barrier discharge reactor. Journal of Industrial and Engineering Chemistry. 2014;**20**(5):2761

[47] Zhang H, Li K, Shu C, et al. Enhancement of styrene removal using a novel double-tube dielectric barrier discharge (DDBD) reactor. Chemical Engineering Journal. 2014;**256**:107

[48] Jiang N, Lu N, Shang K, et al. Innovative approach for benzene degradation using hybrid surface/packed-bed discharge plasmas. Environmental Science & Technology. 2013;**47**(17):9898

[49] Conrads H, Schmidt M. Plasma generation and plasma sources. Plasma Sources Science and Technology. 2000;**9**:441-454

[50] Jingfeng T, Liqiu W, Nan L, et al. Repetitive nanosecond volume diffuse discharge under airflows. IEEE Transactions on Plasma Science. 2014;**42**(3):1-5

[51] Jingfeng T, Liqiu W, Yuxin H, et al. Effect of airflows on repetitive nanosecond volume discharges. IEEE Transactions on Plasma Science, Plasma Science and Technology. 2016;**18**(3):273-277